JOURNAL OF PROPULSION AND POWER
Vol. 29, No. 1, January–February 2013

Solid-Fuel Regression Rate Modeling for Hybrid Rockets

F. M. Favaró* and W. A. Sirignano†
University of California, Irvine, Irvine, California 92697
and
M. Manzoni‡ and L. T. DeLuca§
Politecnico di Milano, 20156 Milan, Italy

DOI: 10.2514/1.B34513

The regression rate of the solid fuel is a primary parameter in the performance analysis for a hybrid rocket. Many studies in the past few years have theoretically claimed, or experimentally shown, a dependence of the regression rate on the chamber total pressure. Such behavior is generally traced back to the presence of oxygen below the flame zone and of heterogeneous reactions occurring at the surface and affecting the pyrolysis law. An experimental program was performed at the Space Propulsion Laboratory of the Politecnico di Milano showing, within the explored operating conditions and the associated uncertainty bands, a neutral trend for the solid fuel regression rate with increasing pressure. The formulation tested was hydroxyl-terminated polybutadiene in gaseous oxygen at pressures ranging from 4 to 16 bar. A simplified analytical model, which retains the essential physics and accounts for pressure dependency, has been developed, together with the corresponding numerical simulation. The results of the proposed model are presented here. The experimental results are input to the developed model, to obtain a semi-empirical pyrolysis rate law that helps to describe a possible pressure dependency.

Nomenclature

B_{TD}	=	preexponential constant, mm/s
c_p	=	specific heat, J/kg · K
D	=	port diameter, mm
E	=	activation energy, kcal/mol
$E(T_s)$	=	generalized energy per unit mass, J/kg
f	=	generic function
G_{ox}	=	specific oxidizer mass flux, kg/(m^2 · s)
H	=	energy per unit mass, J/kg
k	=	slope of viscosity's linear correlation, m/s
$\dot{m}$	=	constant mass flow, kg/s
p	=	pressure, bar
$\dot{Q}$	=	heat flux, W/m^2
R	=	universal gas constant, kcal/mol
Re	=	Reynolds number
$\dot{r}$	=	solid-fuel regression rate, mm/s
S	=	superscalar constant, J/kg
T	=	temperature, K
t	=	time, s
u	=	horizontal velocity, m/s
Y	=	mass fraction
α	=	thermal diffusivity, m^2/s
α_1	=	conserved scalar
α_2	=	conserved scalar, J/kg
β	=	slope of boundary layer's linear correlation
γ	=	slope of flame position's linear correlation
δ	=	boundary-layer thickness, m
δ^*	=	flame position, m
η	=	similarity variable
λ	=	thermal conductivity, W/(m · K)
μ	=	mixture oxidizer-to-fuel ratio
ν	=	kinematic viscosity, m^2/s
ρ	=	density, kg/m^3

Subscripts

comb	=	combustion
f	=	fuel
fl	=	flame
g	=	gas
ox	=	oxygen
o	=	standard condition
pyr	=	pyrolysis
s	=	surface
st	=	stoichiometric
t	=	turbulent
∞	=	freestream

Introduction

THE hybrid rocket is potentially important because it has the promise of combining many of the advantages of both liquid and solid rockets. The simplicity of a solid rocket is in fact merged with the controllability and safety of a liquid one. The hybrid rocket also shows a high degree of flexibility regarding the type of fuel used and the promise of significant savings in the development and management costs. Unfortunately, though hybrid-rocket combustion and propulsion characteristics have been investigated for more than six decades, practical motor development and maturation has not been as actively pursued as that of liquid- and solid-rocket engines. Classical hybrids suffer from many deficiencies: starting from low regression rates (at least an order of magnitude lower than those of a solid rocket), to poor combustion efficiency (due to the fact that, in a hybrid rocket, the oxidizer and fuel mixing occurs on a macroscopic scale), through the general difficulty of operating large-scale engines. There is also the possibility of significant longitudinal instabilities during operation, and it is worth considering the fact that, in general, the mixture ratio will change in time.

A deeper understanding of the phenomena governing the solid-fuel regression rate and the combustion process of the hybrid rocket could lead to a better comprehension of the reasons determining its performance limits. The classical hybrid-motor combustion model, developed by Marxman and Wooldridge [1] and Gilbert and

Received 19 November 2011; revision received 20 May 2012; accepted for publication 10 June 2012; published online 19 December 2012.

*Graduate Student Researcher, Mechanical and Aerospace Engineering Department.

†Professor, Mechanical and Aerospace Engineering Department. AIAA Fellow.

‡M.Sc. candidate, Aerospace Engineering Department, Space Propulsion Laboratory.

§Professor, Aerospace Engineering Department, Space Propulsion Laboratory. AIAA Associate Fellow.

Marxman [2] in the early 1960s, is based on turbulent boundary-layer transport mechanisms with a diffusion-limited combustion process. Their earlier model did not predict any effect of pressure (or mass fraction of reactive species coming from the oxidizer flow) on the solid-fuel regression rate. Actually, the process is considered to be slightly sensitive to the operating conditions, as the macroscopically diffusive flame is controlled by fluid dynamic laws rather than by chemical kinetics. The regression of the solid surface is sustained by the thermal energy feedback from the flame, resulting in a purely convective model. Those studies led to the generation of a family of regression rate laws in the form $\dot{r} = f(x)G_{ox}^{n}$ with an exponent of about $n \approx 0.8$.

A few years later, in the early 1970s, Price and Smoot [3] began to theorize the possibility of a dependence between the solid-fuel regression rate and the operating conditions of the chamber. Their analysis, resulting from intensive experimental studies, showed that the exponent, for the specific oxidizer mass flux G_{ox}, varied not only depending on the value of the same mass flow, but also with changes in the total chamber pressure. Although their early studies showed an enhancement of the regression rate with increasing pressure (assuming a fixed value of the local mass flow), the authors failed to find a satisfactory theoretical explanation for the results. In a subsequent work [4], the authors conjectured that this cause was to be found in the presence of oxygen at the solid surface. That led to the occurrence of heterogeneous reactions between the solid fuel and the surrounding gaseous oxygen, making the solid interface more reactive. One of the major conclusions was that the assumed dependence on the chamber pressure increased as the local specific mass flux increased. However, even though several arguments were proposed in favor of this hypothesis [4], a proved explanation for the witnessed behavior was still missing. One of the rejected explanations regarded the radiative heat flux increase with pressure. For high-mass flows, when the thermal radiation is negligible compared with convection, the pressure dependence should be weak. Conversely, for small-mass flows, the convective heat transfer should become negligible, leading to the independence of the rate of regression on the mass flow and to a considerable change with pressure. Hence, the influence of heat exchanged by radiation would have an opposite effect to that found in the experimental activity and was therefore rejected by Price and Smoot. Moreover, in nonmetalized fuel grains, such as those considered in this work, at pressures and flux levels of interest for propulsion applications, the heat transferred by convection should be much larger than that transferred by gas-phase radiation or radiation from soot particles in the flow [5]. As a result, the basic characteristics of fuel grain regression may, and will, be explored via an analysis of convective heat transfer in a turbulent boundary layer.

It was only after the 1990s that the inquiry of the dependence on chamber operating conditions was resumed. Two research groups at the University of Delaware and Pennsylvania State University have separately conducted some important analysis. The first one, led by Arisawa and Brill, studied in detail the pyrolysis of hydroxyl-terminated polybutadiene (HTPB) [6,7]. The products resulting from the fuel sublimation were analyzed in different conditions of pressure and heating rate of the polymer. The study shows that, below a certain temperature, the pyrolysis process is governed by the decomposition of the solid matrix (and thus by the rate of formation of gasses from sublimated fuel), whereas, above it, the evolution of the gas mixture is controlled by the rate of desorption of gaseous species. They argue that the effect of pressure increase is to lower the transition temperature between the two phenomena. In this sense, seeing the pyrolysis process as a kind of evaporation, the pressure increases to the detriment of the gas desorption from the solid matrix. This is confirmed by the fact that, for higher pressures, the molecules of gas produced are smaller, and the production of monomers is favored over that of oligomers.

The second group, composed of Risha et al. [8], reports the only evidence in the literature of an actual decrease of the regression rate with pressure. An empirical law that has a strong dependence on the pressure is also fitted:

$$\dot{r} = 3.02(Y_{O_2} - 0.21)^{0.19} T_{ox}^{1.28} \frac{\dot{m}_{ox}^{0.5}}{p^{0.43}} \quad (1)$$

Here, Y_{O_2} represents the freestream oxygen mass fraction. Another law, in the form of Arrhenius, is also presented and it will be used in the following. The article states that, in the presence of chemically reactive species, the pyrolysis of many polymers is greatly accelerated. The increase in the thermal degradation of the surface in contact with oxygen is caused by three main factors: the absorption of oxygen by the solid, which changes the structure of the polymer and alters its mechanism of decomposition; exothermic heterogeneous reactions on the surface; and heat transfer due to homogeneous reactions between oxygen and pyrolysis products. The final effect of all of these overlapping processes is not easily predictable.

Although none of the analyzed studies present a conclusive theoretical explanation of the phenomena at stake, many of the reported data were used for the parameters setting of the following model and, therefore, support the development of this research.

Experimental Activity

The purpose of the testing was to determine whether there is a pressure dependence of the regression rate for nonmetalized hybrid-fuel systems. If so, further theoretical studies would help to understand the causes and develop a model of such a behavior. Several tests were conducted at the Space Propulsion Laboratory at Politecnico di Milano, testing HTPB in gaseous oxygen (GOX) at increasing pressure values.

To acquire a better understanding of the effects of the operating conditions on the regression rate of the tested fuel, for each test, a fuel sample was placed in a windowed combustor under controlled operating conditions. The combustor was sealed and brought to a selected pressure level using a continuous purge of nitrogen gas. GOX was then introduced into the combustor to burn with the pyrolysis products generated from the fuel sample. The experimental line is presented in Fig. 1.

The method of ignition used to start the combustion process was an external radiative energy flux from a high-powered CO_2 laser. Around 40 tests were conducted under the following operating conditions: 1) pressure ranged from 4 to 16 bar (58–232 psi); 2) oxidizer injection temperature was 298 K; 3) oxidizer mass flow rate (100% GOX) was kept constant at the value of 5 g/s [210 normal liters per minute (nlpm)]; and 4) a cured HTPB fuel formulation was tested.

Experimental Setup

To operate the test system, three types of control panels were used: one for controlling the oxidizer mass flow; one for the pressurizing system N_2 connected to a differential manometer and to the electrovalves for the chamber pressure control; and one for a

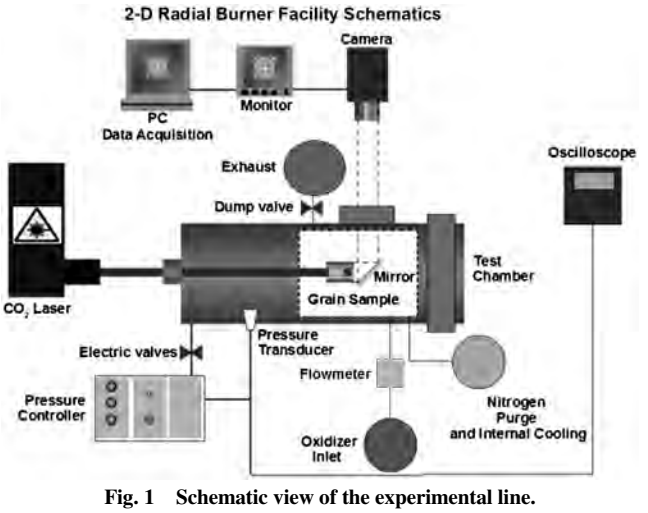

Fig. 1 Schematic view of the experimental line.

Fig. 2 HTPB cylindrical sample showing central perforation (left) and ignition charge (right).

computerized data acquisition. The signal from the high-resolution pressure transducer was monitored and used to adjust the exhaust valve opening to maintain constant the preselected combustor pressure. The data recorded were used to verify that the pressure in the combustor remained nearly constant during the test. The control panels were positioned far enough from the combustor to ensure safe operation.

The combustor was designed with a continuous purge for constant pressure combustion up to 30 bar (441 psi). The feeding mechanism and the head of the combustor are capable of handling cylindrical samples of 20 mm in external diameter and a length of 30 mm, with a circular central port of 4 mm initial diameter. This small burner is contained in a metallic case of about 35 cm in length and 15 cm in diameter. Pictures of the cylindrical sample are reported in Fig. 2.

The combustor case is equipped with two windows ports: one for the camera recording the motion picture of the combustion and one for the laser entrance. An example of this procedure is shown in Fig. 3. The radiant energy flux from the high-powered CO_2 laser was supplied directly to an initiator located at the top of the fuel sample (inside a cylindrical port, also visible in Fig. 2); this method ensures that the ignition of the solid-fuel surface is as uniform as possible. A zinc selenide cylinder doped with chromium (ZnSe:Cr) has been used as an infrared transparent window. Two different cameras were used: a XYBION SVC-09 equipped with a MOS-485 × 376 sensor able to collect 25 frames per second (fps) and a Photron with CMOS-1024 × 1024 sensor able to collect 500 fps. Changes in video frame rate did not affect the regression rate values measured. The videos were instantly compressed and saved on an external hard drive.

Regression Rate Determination

For each value of pressure in the considered range, at least four trials with their recordings were considered. In this way, it is possible to measure the instantaneous variation of the mean port diameter yielding the instantaneous regression rate.

Each video was processed with a frame analysis program. In this case, the RedLake Imaging Motion Scope software CAMERA was used. The video was then scrolled frame by frame to capture the variation of the port diameter with time. This was done using a pixel reticle that enabled, for each frame, the capture of a suitable number of diameters to correctly describe the regressing surface. A software package able to automatically detect the regressing surface was also used to analyze the combustion video recordings. In the case of pure HTPB, automatic processing yielded essentially the same results as the manual processing, of course taking much less time, while providing many more data. The manual procedure, however, is expected to be of broader validity because it can also be applied to solid fuels whose regression surface is obscured by a variety of noise sources (observed with high-energy additives), irregularities and anisotropies (observed with wax-based samples), and peculiar phenomena (solid-fuel fragmentation) not easily captured by an automatic software.

The measure of the port diameter change with time was then converted into millimeters (from the original pixel data) with a calibration of the camera. The history of diameter variation was interpolated in the form

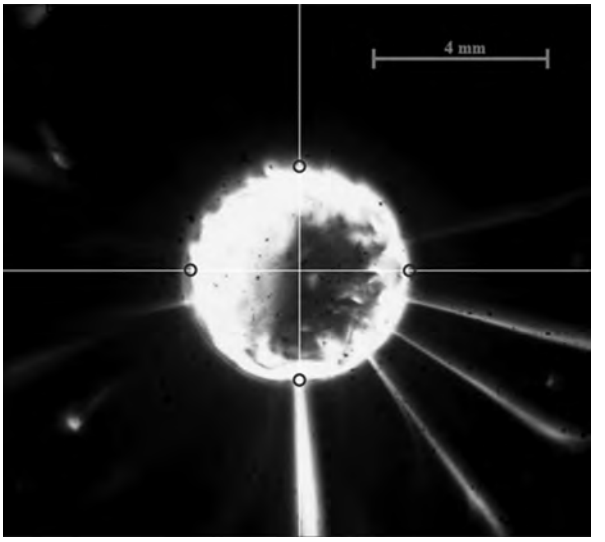

Fig. 3 Frame from a combustion video recording showing the sample burning port. The small circles indicate the regression surface position.

$$D - D_o = f(t) = a \cdot t^n \tag{2}$$

The regression rate is then easily calculated by a simple time differentiation:

$$\dot{r} = \frac{\mathrm{d}(D(t)/2)}{\mathrm{d}t} = b \cdot t^m \tag{3}$$

so that $b = 0.5a \times n$ and $m = n - 1$. Knowing the variation of the port diameter, it is possible to also deduce the specific mass flow in time as

$$G_{\mathrm{ox}} = \frac{\dot{m}_{\mathrm{ox}}}{\pi[D(t)^2/4]} \equiv \frac{\dot{m}_{\mathrm{ox}}}{\pi[(D_o + at^n)^2/4]} \tag{4}$$

from which data are interpolated to find a law in the form

$$\dot{r} = cG_{\mathrm{ox}}^q \tag{5}$$

The results obtained for all the trials are reported in Fig. 4, which shows the instantaneous regression rate as a function of the oxidizer mass flux G_{ox}.

The results shown in Fig. 4 do not highlight a clear trend of the regression rate as a function of pressure. To get such an explicit trend of the regression rate as a function of the specific mass flow and pressure, it is necessary to get one single curve for each pressure

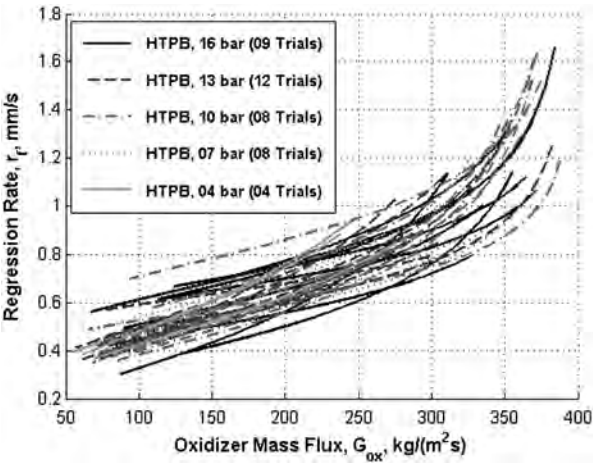

Fig. 4 Comparison of instantaneous regression rate for all the tests showing similar trends for all experimental curves within the explored operating conditions (210 nlpm flow of oxygen was used).

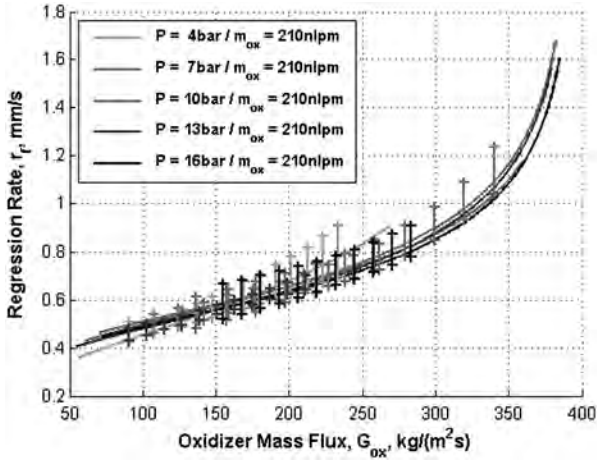

Fig. 5 Instantaneous ensemble regression rate showing negligible pressure dependence within the explored operating conditions.

value. This is done by means of the same interpolation explained before, where the N curves in the form of Eq. (2) (where N is the number of tests), are replaced by one single curve, obtained from the interpolation of all the data coming from different tests at the same pressure. It is then possible to plot the instantaneous regression rate r_f versus the specific oxidizer mass flux G_{ox}. Results are shown in Fig. 5.

A significant pressure dependency of the regression rate is not observed. Previous works [9–11] have established a weak dependence of the regression rate on pressure. In agreement with previous studies [3], other trends are possible. Note that, except for the research at Pennsylvania State University, trials at high pressures ($p \geq 10$ bar) with larger amounts of fuel in the chamber were not found in the literature (or, at least, not testing pure HTPB).

Risha et al. [8] tested HTPB in N_2/O_2 oxidizer (with the oxygen mass fraction going from 0.21 to 1) and found that the regression rate increased with freestream oxygen mass fraction, oxidizer mass flow rate, and oxidizer temperature. However, it decreased with increasing chamber pressure. They collapsed the solid-fuel regression rate into a single line using multivariable regression analysis with the power law of Eq. (1), where a significant pressure dependence is witnessed. It is not possible to perceive such a clear trend from the results of Fig. 5 of the experimental campaign carried out at the Space Propulsion Laboratory. Two main differences are to be noted: the Pennsylvania State experimental campaign used an end burner combustor and, also, the proposed law is computed for laminar conditions.

The following analytical model is intended to be able to account for various observed trends of the regression rate. It should provide a solid base for the development of a new regression rate law that could explain a possible pressure dependency. The goal is to retain the essential physics in the most simplified form. We aim to explain pressure dependence and not to reproduce all details of the flowfield. However, given the relevance that a study like the preceding [8] carries, the regression rate proposed by Pennsylvania State University will also be tested in the analytical model.

Comprehensive Analytical Model

A simplified model for the boundary layer that surrounds the cylindrical solid fuel is presented here. Given empirical input for a pyrolysis law, it will yield analytical values for the temperature at the surface and at the flame and for the regression rate. The other unknowns of the model will be the fuel and oxidizer mass fractions and the flame position. The oxygen will, in general, be allowed to diffuse below the flame zone because it is believed to be the major cause for the possible dependence on operating conditions.

Realize that no model can be developed without an empirical representation of one particular process, namely the pyrolysis. We expect the pyrolysis rate might have explicit pressure dependence, as well as the temperature and concentration dependences. Furthermore, there can be implicit pressure dependence through the temperature and concentration variables. The analytical representation of the flow and transport physics is required to separate the implicit and explicit dependences on pressure.

Our steady-state model will equate mass burning rates and mass pyrolysis rates with each other and proportion them with the regression rate; mass pyrolysis rate per unit surface area will equal solid-phase density times the surface regression rate. The pyrolysis rate will depend on surface temperature, pressure, and concentrations, whereas those values depend on the behavior of the field, including gas and solid phases. Therefore, determination of the magnitudes of pyrolysis, burning, and regression rates will depend upon the system constraints. The flame that stands at some distance off the gas–solid interface will be assumed to be diffusion controlled. Transport of mass and energy will be represented analytically, accounting for turbulent mixing in the gas. The pyrolysis-rate law will be determined by matching the theoretical prediction to our experimental results.

Figure 6 shows a schematic of the simplified model that will be used in the following development of the equations for the turbulent-boundary-layer model. The main assumptions are as follows:

1) The thickness of the turbulent boundary layer δ and the transverse position of the flame δ^* are considered linearly dependent on x, as common in turbulent boundary layers:

$$\delta = \delta(x) = \beta x; \qquad \delta^* = \delta^*(x) = \gamma x \tag{6}$$

2) The slope β is an assigned constant (the development of the boundary layer is known), and γ is unknown.

3) The solid-fuel regression rate is considered uniform in the x direction.

4) The diffusion layers in the gas and solid are sufficiently thin compared with the chamber diameter to allow a two-dimensional approximation.

5) We consider $Pr = Le = Sc = 1$ in the turbulent condition. This will allow the interchange of α_t, ν_t, and D_t, respectively, thermal diffusivity, kinematic viscosity, and mass diffusivity.

6) The transverse velocity and the streamwise diffusion are neglected.

7) Low Mach number is assumed.

8) All the properties of the fuel (α_f, ρ_f, c_{p_f}, and λ_f) will be considered uniform in the solid.

9) Infinite oxidation kinetic rates are assumed, so that a thin flame results with no dissociation of products.

10) The turbulent kinematic viscosity is assumed linearly proportional to the x variable, because turbulent eddy size grows with downstream distance:

$$\nu_t = \nu_t(x) \propto kx \tag{7}$$

The variable k may follow different trends, but it is assumed that the ratio u/k remains constant.

Three different domains are considered: two gaseous domains above and below the flame, and a third domain within the solid fuel. For the two gaseous domains, the diffusion equations for mass and energy are written, whereas in the solid domain, a conduction problem (in y direction) for a semi-infinite slab, with the surface in vertical

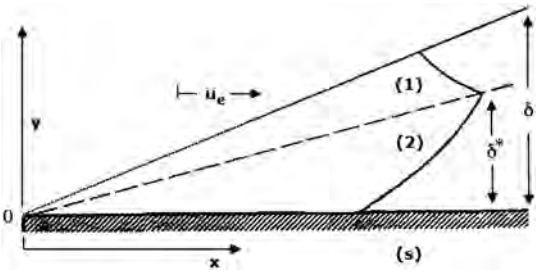

Fig. 6 Schematic representation of the temperature profile in the turbulent boundary layer over the fuel slab.

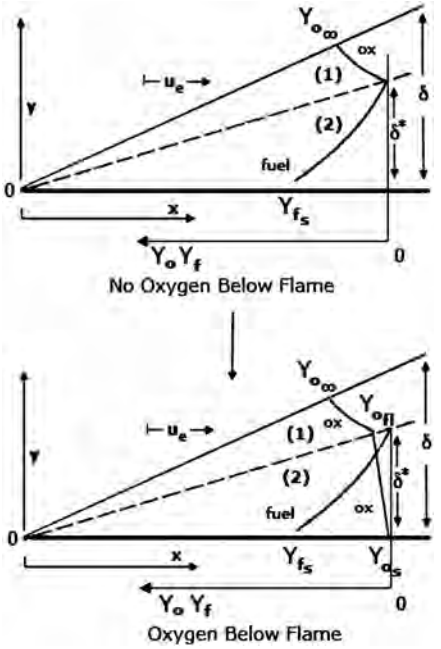

Fig. 7 Schematic representation of the profiles inside the boundary layer.

motion at a velocity equal to the regression rate, is considered. Schematic representations of the mass fraction profiles are given in Fig. 7. Given the assumptions described in the three domains, the global problem for the oxidizer mass fraction can be stated as

$$u\frac{\partial Y_o}{\partial x} = D_t\frac{\partial^2 Y_o}{\partial y^2}; \qquad Y_o(x,\delta) = Yo_\infty \tag{8}$$

The values at the flame $Y_o(x,\delta^*) \equiv Yo_{\rm fl}$ and at the surface $Y_o(x,0) \equiv Yo_s$ remain to be determined. For the fuel vapor,

$$u\frac{\partial Y_f}{\partial x} = D_t\frac{\partial^2 Y_f}{\partial y^2}; \qquad Y_f(x,\delta^*) = 0 \tag{9}$$

where $Y_f(x,0) \equiv Y_{f_s}$ and δ^* remain to be determined and no fuel overreaches the flame zone. For the energy,

$$u\frac{\partial T}{\partial x} = \alpha_t\frac{\partial^2 T}{\partial y^2}; \qquad T(x,\delta) = T_\infty \tag{10}$$

Here, $T(x,\delta^*) \equiv T_{\rm fl}$ and $T(x,0) \equiv T_s$ remain to be determined. Within the solid domain, $y \le 0$, the temperature is governed by

$$\frac{\lambda_f}{\rho_f c_p}\frac{{\rm d}^2T}{{\rm d}y^2} - \dot r\frac{{\rm d}T}{{\rm d}y} = 0; \qquad T(x,-\infty) = T_o \tag{11}$$

with the temperature matching T_s at $y = 0$.

Similar solutions are found in the gas phase with $\eta = y/x$. The coordinate transformation causes Eqs. (8–10) to be replaced by ordinary differential equations

$$L(Y_o) \equiv \frac{{\rm d}^2Y_o}{{\rm d}\eta^2} + \frac{u}{k}\eta\frac{{\rm d}Y_o}{{\rm d}\eta} = 0 \tag{12}$$

$$L(Y_f) = 0 \tag{13}$$

$$L(T) = 0 \tag{14}$$

with matching conditions at $\eta = 0$ (surface) and $\eta = \gamma$ (flame). The solutions for domain 1, as shown in Fig. 6, are given by

$$Y_{o_{(1)}} = \frac{(Y_{o_{\rm fl}} - Y_{o_\infty})[{\rm erf}(\eta\sqrt{u/2k}) - {\rm erf}(\beta\sqrt{u/2k})]}{[{\rm erf}(\gamma\sqrt{u/2k}) - {\rm erf}(\beta\sqrt{u/2k})]} + Y_{o_\infty} \tag{15}$$

$$\frac{{\rm d}Y_{o_{(1)}}}{{\rm d}\eta} = \sqrt{\frac{2u_\infty}{k\pi}}\frac{(Y_{o_{\rm fl}} - Y_{o_\infty})}{[{\rm erf}(\gamma\sqrt{u/2k}) - {\rm erf}(\beta\sqrt{u/2k})]}e^{-\frac{\eta^2 u_\infty}{2k}} \tag{16}$$

$$Y_{f_{(1)}} = 0 \tag{17}$$

$$\frac{{\rm d}Y_{f_{(1)}}}{{\rm d}\eta} = 0 \tag{18}$$

$$T_{(1)} = \frac{(T_{\rm fl} - T_\infty)[{\rm erf}(\eta\sqrt{u/2k}) - {\rm erf}(\beta\sqrt{u/2k})]}{[{\rm erf}(\gamma\sqrt{u/2k}) - {\rm erf}(\beta\sqrt{u/2k})]} + T_\infty \tag{19}$$

$$\frac{{\rm d}T_{(1)}}{{\rm d}\eta} = \sqrt{\frac{2u_\infty}{k\pi}}\frac{(T_{\rm fl} - T_\infty)}{[{\rm erf}(\gamma\sqrt{u/2k}) - {\rm erf}(\beta\sqrt{u/2k})]}e^{-\frac{\eta^2 u_\infty}{2k}} \tag{20}$$

For domain 2 of Fig. 6, we obtain

$$Y_{o_{(2)}} = \frac{(Y_{o_{\rm fl}} - Y_{o_s})}{{\rm erf}(\gamma\sqrt{u/2k})}{\rm erf}\left(\eta\sqrt{\frac{u}{2k}}\right) + Y_{o_s} \tag{21}$$

$$\frac{{\rm d}Y_{o_{(2)}}}{{\rm d}\eta} = \sqrt{\frac{2u_\infty}{k\pi}}\frac{(Y_{o_{\rm fl}} - Y_{o_s})}{{\rm erf}(\gamma\sqrt{u/2k})}e^{-\frac{\eta^2 u_\infty}{2k}} \tag{22}$$

$$Y_{f_{(2)}} = \frac{-Y_{f_s}}{{\rm erf}(\gamma\sqrt{u/2k})}{\rm erf}\left(\eta\sqrt{\frac{u}{2k}}\right) + Y_{f_s} \tag{23}$$

$$\frac{{\rm d}Y_{f_{(2)}}}{{\rm d}\eta} = \sqrt{\frac{2u_\infty}{k\pi}}\frac{-Y_{f_s}}{{\rm erf}(\gamma\sqrt{u/2k})}e^{-\frac{\eta^2 u_\infty}{2k}} \tag{24}$$

$$T_{(2)} = \frac{(T_{\rm fl} - T_s)}{{\rm erf}(\gamma\sqrt{u/2k})}{\rm erf}\left(\eta\sqrt{\frac{u}{2k}}\right) + T_s \tag{25}$$

$$\frac{{\rm d}T_{(2)}}{{\rm d}\eta} = \sqrt{\frac{2u_\infty}{k\pi}}\frac{(T_{\rm fl} - T_s)}{{\rm erf}(\gamma\sqrt{u/2k})}e^{-\frac{\eta^2 u_\infty}{2k}} \tag{26}$$

For the solid-fuel domain, the solution is

$$T = T_o + (T_s - T_o)e^{\frac{\dot r}{\alpha_f}y} \tag{27}$$

$$\frac{{\rm d}T}{{\rm d}y} = \frac{\dot r}{\alpha_f}(T_s - T_o)e^{\frac{\dot r}{\alpha_f}y} \tag{28}$$

There are seven unknowns of the problem ($\dot r$, T_s, $T_{\rm fl}$, $\delta^* \to \gamma$, Y_{f_s}, Y_{o_s}, and $Y_{o_{\rm fl}}$). For the special case in which no oxygen is consumed at the surface, $Y_{o_{\rm fl}} = Y_{o_s} = 0$ and only five unknowns are left.

Matching Conditions at Flame and Surface

In general, it is necessary to write seven matching equations between the given profiles, at the flame, and at the surface. The resulting algebraic system will be numerically solved as highly

nonlinear. In the following equations, $\dot{m}$ is the mass flow per unit area, μ represents the mixture ratio, and λ is the thermal conductivity in [watts/(meter*degree Kelvin)]. T, Y_o, and Y_f are continuous at the flame, although the derivatives are discontinuous. Similarly, T is continuous at the solid interface, whereas its derivative is discontinuous there.

1) Stoichiometric condition at the flame $y = \delta^*$:

$$\frac{\partial Y_{o_{(2)}}}{\partial y} - \frac{\partial Y_{o_{(1)}}}{\partial y} = \mu_{\text{st}} \frac{\partial Y_{f_{(2)}}}{\partial y} \tag{29}$$

2) Energy balance at the flame $y = \delta^*$:

$$\lambda_{(2)} \frac{\partial T_{(2)}}{\partial y} - \lambda_{(1)} \frac{\partial T_{(1)}}{\partial y} = \dot{Q}_{\text{comb}} = -D_t \rho_{\text{fl}} H_{\text{fl}} \frac{\partial Y_{f_{(2)}}}{\partial y} \tag{30}$$

3) Energy balance at the surface $y = 0$:

$$\left(\lambda_g \frac{\partial T_{(2)}}{\partial y} - \dot{m} c_{p_g} T_s\right) - \left(\lambda_f \frac{\partial T_{(s)}}{\partial y} - \dot{m} c_{p_f} T_s\right) = -\dot{Q}_{\text{pyr}} = -H_{\text{pyr}} \rho_f \dot{r} \tag{31}$$

4) Mass balance at the interface $y = 0$:

$$\dot{m}_g \equiv \dot{m} = \dot{m} Y_{o_s} + \dot{m} Y_{f_s} - \rho_g D_t \frac{\partial Y_f}{\partial y}\Big|_s - \rho_g D_t \frac{\partial Y_o}{\partial y}\Big|_s = \rho_f \dot{r} \tag{32}$$

5) Stoichiometric condition at the interface $y = 0$:

$$\mu_{\text{pyr}} \rho_f \dot{r} = \rho_g D_t \frac{\partial Y_o}{\partial y}\Big|_s - \dot{m} Y_{o_s} \tag{33}$$

Conditions 4 and 5 imply that

6)

$$-\frac{\mu_{\text{pyr}}}{1 + \mu_{\text{pyr}}} = \frac{\dot{m}_{\text{ox}}}{\dot{m}_f} = \frac{-\rho_g D_t (\partial Y_{o_{(2)}}/\partial y) + \rho_s \dot{r} Y_{o_{(2)}}}{-\rho_g D_t (\partial Y_{f_{(2)}}/\partial y) + \rho_s \dot{r} Y_{f_{(2)}}} \tag{34}$$

Condition 6 can be applied at the flame location to help determine the unknowns. To solve the system, we need one final equation that models the behavior of the pyrolysis rate at the surface:

7) Pyrolysis law at $y = 0$.

As a start, such a law will be modeled with

$$\dot{r} = B_{TD}(1 + cY_{o_s}) \exp\left(-\frac{E_{TD}}{RT_s}\right) \tag{35}$$

Note that, for generality, Eq. (35) is a slightly modified version of the pyrolysis rate law found by the Pennsylvania State University research group in [8]. It contains, inside the preexponential factor B_{TD}, the experienced pressure dependence, if any. Such a relation will be replaced in a later section by the semi-empirical law given in Eq. (60). Also note that, when no oxygen reaches the surface, conditions 5 and 6 are not applicable, Eq. (35) assumes the form proposed in [8], and Y_{o_s} and $\partial Y_o/\partial y|_s$ become zero in Eq. (32).

Conserved Scalar Approach

We now use the conserved scalars of the problem, which will greatly simplify the equations. In fact, in this way, it is possible to separate the problem at the flame (in terms of temperature and position) from the other unknowns. To rework the system, it is possible to define two Shvab-Zel'dovich variables [12]:

$$\alpha_1 = Y_o - \mu_{\text{st}} Y_f \tag{36}$$

$$\alpha_2 = c_p T + H_{\text{fl}} Y_f \tag{37}$$

that satisfy the general problem

$$u \frac{\partial \alpha}{\partial x} = \nu \frac{\partial^2 \alpha}{\partial y^2} \tag{38}$$

where only the boundary conditions at the wall and outside the boundary layer are required because the two variables are continuous through the flame, both being monotonic. In addition, a linear combination of these variables yields a superscalar S [12], which is a constant quantity throughout the domain. Considering, in fact, the derivative of α_1 and α_2 at the surface

$$\frac{\partial \alpha_1}{\partial y}_{|_s} = \frac{\partial Y_o}{\partial y}_{|_s} - \mu_{\text{st}} \frac{\partial Y_f}{\partial y}_{|_s} \tag{39}$$

and

$$\frac{\partial \alpha_2}{\partial y}_{|_s} = c_p \frac{\partial T}{\partial y}_{|_s} + H_{\text{fl}} \frac{\partial Y_f}{\partial y}_{|_s} \tag{40}$$

$S_\infty = S_s$Inserting the given profiles, it is possible to find the following relation:

$$\frac{\partial \alpha_2}{\partial y}_{|_s} - \frac{[E(T_s) - H_{\text{fl}}(1 + \mu_{\text{pyr}} - Y_{f_s})]}{(\mu_{\text{pyr}} + Y_{o_s}) + \mu_{\text{st}}(1 + \mu_{\text{pyr}} - Y_{f_s})} \frac{\partial \alpha_1}{\partial y}_{|_s} = 0 \tag{41}$$

where $E(T_s) = c_{p_f}(T_s - T_o) - H_{\text{pyr}} + T_s(c_{p_g} - c_{p_f})$ represents the total energy per unit mass of fuel at the surface. Equations (38) and (41) imply that the quantity

$$S = \alpha_2 + \frac{[H_{\text{fl}}(1 + \mu_{\text{pyr}} - Y_{f_s}) - E(T_s)]}{(\mu_{\text{pyr}} + Y_{o_s}) + \mu_{\text{st}}(1 + \mu_{\text{pyr}} - Y_{f_s})} \alpha_1 \tag{42}$$

is a constant. From now on, this quantity will be referred to as a superscalar. The superscalar (or supervariable) S is a combination of the primitive dependent variables and becomes uniform over the space. More information regarding the use of superscalars can be found in [12]. Two equations are then given by the equalities $S_{\text{fl}} = S_\infty$ and $S_\infty = S_s$, a third one by the pyrolysis law in the Arrhenius form previously presented. Two more equations are derived by comparing the first derivatives of α_1 and α_2 by definition with those derived from the solution of Eq. (38). The use of the superscalar at the surface and the flame can replace two of the balance conditions because it was constructed using those conditions. Finally, the mass balance at the wall is considered, whereas the position of the flame can be calculated from the observation that $\alpha_1(\gamma) \equiv Y_{o_{\text{fl}}}$. The final system of seven equations is given by

$$c_p(T_{\text{fl}} - T_\infty) + \frac{[H_{\text{fl}}(1 + \mu_{\text{pyr}} - Y_{f_s}) - E(T_s)]}{(\mu_{\text{pyr}} + Y_{o_s}) + \mu_{\text{st}}(1 + \mu_{\text{pyr}} - Y_{f_s})}(Y_{o_{\text{fl}}} - Y_{o_\infty}) = 0 \tag{43}$$

$$c_p(T_s - T_\infty) + H_{\text{fl}} Y_{f_s} + \frac{[H_{\text{fl}}(1 + \mu_{\text{pyr}} - Y_{f_s}) - E(T_s)]}{(\mu_{\text{pyr}} + Y_{o_s}) + \mu_{\text{st}}(1 + \mu_{\text{pyr}} - Y_{f_s})}(Y_{o_s} - \mu_{\text{st}} Y_{f_s} - Y_{o_\infty}) = 0 \tag{44}$$

$$\frac{Y_{o_\infty} - Y_{o_s} + \mu_{\text{st}} Y_{f_s}}{\text{erf}(\beta\sqrt{u/2k})} \sqrt{\frac{2u_\infty}{k_1 \pi}} = \frac{\rho_f \dot{r}}{\rho_g k_2}[(\mu_{\text{pyr}} + Y_{o_s}) + \mu_{\text{st}}(1 + \mu_{\text{pyr}} - Y_{f_s})] \tag{45}$$

$$\frac{c_p(T_\infty - T_s) - H_{\text{fl}} Y_{f_s}}{\text{erf}(\beta\sqrt{u/2k})}\sqrt{\frac{2u_\infty}{k_1\pi}} = \frac{\rho_f \dot{r}}{\rho_g k_2}[E(T_s) - H_{\text{fl}}(1 + \mu_{\text{pyr}} - Y_{f_s})] \tag{46}$$

$$\dot{r} = B_{TD}(1 + cY_{o_s})e^{-\frac{E_{TD}}{RT_s}} \tag{47}$$

$$\frac{Y_{o_\infty} - Y_{o_s} + \mu_{\text{st}} Y_{f_s}}{\text{erf}(\beta\sqrt{u/2k})}\text{erf}\left(\gamma\sqrt{\frac{u}{2k}}\right) + (Y_{o_s} - \mu_{\text{st}} Y_{f_s}) = Y_{o_{\text{fl}}} \tag{48}$$

$$\rho_f \dot{r} = \dot{m}Y_{o_s} + \dot{m}Y_{f_s} + \rho_g k_2\sqrt{\frac{2u_\infty}{k_1\pi}}\left[\frac{Y_{f_s} - (Y_{o_{\text{fl}}} - Y_{o_s})}{\text{erf}(\gamma\sqrt{u/2k})}\right] \tag{49}$$

where Eqs. (44–47) provide the solution for the problem at the surface in the unknowns T_s, Y_{o_s}, Y_{f_s}, and $\dot{r}$, whereas the other equations are used to solve the problem at the flame, once the solution at the surface has been gained. In the particular case of no oxygen presence in the second gaseous domain, namely $Y_{o_{\text{fl}}} = Y_{o_s} = 0$, the remaining five unknowns are given by the solution of the following system of equations (50–54):

$$c_p T_{\text{fl}}(1 - Y_{f_s}) = c_p T_s(1 - Y_{f_s}) + E(T_s)Y_{f_s} \tag{50}$$

$$c_p T_{\text{fl}}(1 - Y_{f_s}) = c_p T_\infty(1 - Y_{f_s}) + \frac{H_{\text{fl}}}{\mu_{\text{st}}}Y_{o_\infty}(1 - Y_{f_s}) - \frac{Y_{o_\infty}}{\mu_{\text{st}}}E(T_s) \tag{51}$$

$$\frac{Y_{o_\infty} + \mu_{\text{st}} Y_{f_s}}{\text{erf}(\beta\sqrt{u/2k})}\sqrt{\frac{2u_\infty}{k\pi}} = \frac{\rho_f \dot{r}}{\rho_g k_2}\mu_{\text{st}}(1 - Y_{f_s}) \tag{52}$$

$$\dot{r} = B_{TD}e^{-\frac{E_{TD}}{RT_s}} \tag{53}$$

$$\text{erf}\left(\gamma\sqrt{\frac{u}{2k}}\right) = \frac{\mu_{\text{st}} Y_{f_s}\text{erf}(\beta\sqrt{u/2k})}{Y_{o_\infty} + \mu_{\text{st}} Y_{f_s}} \tag{54}$$

where Eq. (54) comes from the considesration that $\alpha_1(\gamma) = 0$ for this simplified case, and we now consider that

$$\frac{\partial Y_o}{\partial y}_{|_s} = 0 \tag{55}$$

in the definition of the first conserved scalar given by Eq. (36).

Numerical Simulation

Conserved Scalar Approach

The resolution of the system requires a first-guess solution for the iterative process of error minimization, once the system is written in the form $F(x) = 0$. Fortunately, it is not necessary to consider all seven unknowns at one time. In fact, it is possible to note that some of the equations have linear behaviors in some of the unknowns. Nevertheless, the solution is particularly sensitive to the first guess. For this reason, the system resolution is accomplished in a "gradual" way to control the correctness of the outputs of the system for more simple cases.

The conserved scalar approach allows the resolution of two separate problems, making the numerical solution process easier. Not only is it possible to consider the flame position as a separate unknown, but it is not necessary to contain it in the nonlinear system set of unknowns (usually two or three unknowns, depending on whether the presence of oxygen below the flame is considered or not). Considering a constant value of pressure (here, 4 bar) and an assigned linear development of the boundary layer (here, $\beta = 0.102$ coming from the experimental measure of the Reynolds number $Re \approx 9e^4$), it is possible to obtain the results

$$T_s = 789.65 \text{ K}; \qquad Y_{f_s} = 0.862; \qquad T_{\text{fl}} = 2498.4 \text{ K}$$
$$\dot{r} = 0.383 \text{ mm/s}; \qquad \text{erf}\left(\gamma\sqrt{\frac{u}{2k}}\right) = 0.5437 \Rightarrow \gamma = 0.0673$$

using the conserved scalar approach, when no oxygen is considered below the flame. The profiles of the found quantities are shown in dashed lines in Fig. 8. In general, it is expected that, when the oxygen presence below the flame is considered, the surface temperature will increase, at the expense of a decrease in the flame temperature. This is caused by the fact that less oxygen is consumed at the flame (resulting in a nonzero value of $Y_{o_{\text{fl}}}$) because a part of it diffuses below the flame. When considering oxygen, the following solution is found:

$$T_s = 794.99 \text{ K}; \qquad Y_{f_s} = 0.861; \qquad Y_{o_s} = 0.0035$$
$$\dot{r} = 0.475 \text{ mm/s}; \qquad Y_{o_{\text{fl}}} = 0.0337; \qquad T_{\text{fl}} = 2423.6 \text{ K};$$
$$\text{erf}\left(\gamma\sqrt{\frac{u}{2k}}\right) = 0.5501 \Rightarrow \gamma = 0.0683$$

where all seven unknown variables are considered. These results are shown in solid lines in Fig. 8. The higher value of the regression rate can now be related to several different causes. First, the increase in the surface temperature, as explained before, will enhance the values of the exponential in the Arrhenius form of the pyrolysis law of Eq. (35). Also, the value of the preexponential constant is different, whether an inert local environment is considered or oxygen is present at the surface [8,13]. The dependence of law (35) on the oxygen mass fraction at the surface gives a small increase of the regression rate above the value with no oxygen at the solid surface. When considering the presence of oxygen, the flame position is a little higher, as can be seen in Fig. 8.

The cause is an augmented value of the transversal fuel mass injection occurring at the surface, because now the incoming oxygen is added to the solid-fuel flux to give the fuel-vapor flux. Having the flame farther from the surface means that the thermal energy feedback from the flame to the surface is smaller, causing the surface temperature to drop. The higher value of T_s is again attributable to the diffusion of oxygen below the flame because the model is subtracting part of the heat release at the flame, moving it to the surface.

Pressure Dependence

We now consider possible pressure dependencies in the system. This can be done by considering two different types of effects: the

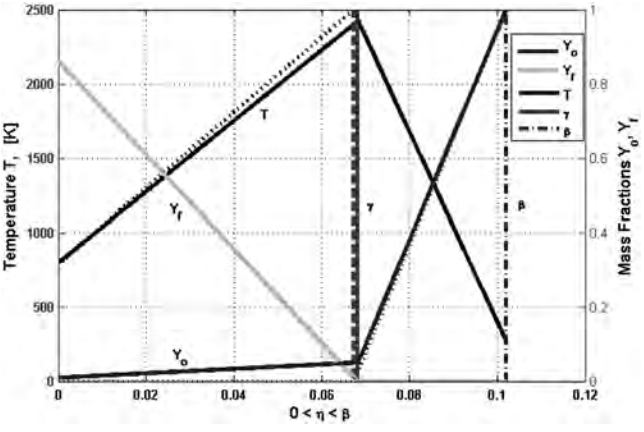

Fig. 8 Oxygen diffusion effects on temperature and mass fraction profiles.

analytical variation of thermodynamic quantities with pressure and the pressure sensitivity of the pyrolysis rate according to empirical descriptions of pyrolysis rate laws found in the literature.

The first effect is the change of the gas density at the surface ρ_s: Inserting the change in the gas density at the surface, through the perfect gas law $\rho_s = p/RT_s$, the regression rate will be increasing with pressure. This is due to an increase in the surface temperature T_s predicted by the model. The temperature rise can in turn be related to the fact that, as the pressure increases, the flame moves toward the surface, enhancing the thermal energy feedback to the solid fuel. The variation with pressure of the kinematic viscosity ν at the wall is also considered. Inside the gaseous domains, this dependence is not taken into account because it is considered that, in the very turbulent regime, this value is very slightly variable. At the solid surface, instead, which is treated as a sublaminar layer, its value is reconnected to the pressure (and temperature) variation through the relation

$$\nu \approx \left[\frac{1}{c_p}(RT)^{3/2}\right]\frac{1}{p} \tag{56}$$

derived from various considerations, arising from chemical kinetics and from the fundamental relations of thermodynamics. Interestingly, this quantity is always present in the equations of the system, multiplied by the density of the gas mixture at the surface. Their product is thus independent of pressure, being the first one directly and the latter inversely proportional to the pressure itself. Thus, nullifying their effect on each other, the profile of the regression rate is at this point dictated solely by the variation with pressure of the preexponential factor B_{TD} in the pyrolysis-rate law. The global effect of the kinematic viscosity is then to cancel the growth of the regression rate due to the density variation. It will also actually bring a more marked dependence on the temperature, which enhances somewhat the value of the regression rate.

The change in the preexponential constant of the pyrolysis-rate law is closely related to the regression rate of the solid fuel. The pyrolysis rate is in fact expressed in the system, in both approaches, with a pyrolysis-rate law in the form of Arrhenius [$\dot{r} = B_{TD}\exp(-E_{TD}/RT_s)$ or $\dot{r} = B_{TD}(1 + cY_{o_s})\exp(-E_{TD}/RT_s)$, depending on whether the presence of oxygen at the wall is denied or not], as previously presented. According to the studies conducted at Pennsylvania State University [8], the preexponential factor of this pyrolysis-rate law is to depend on and, more specifically, to decrease with pressure. From the values given in their work, it is possible to reconstruct a linear law for the variation of this parameter: $B_{TD} = 2.7198 - 0.0634 \times p$ where B_{TD} is given in millimeters per second and the pressure is given in standard atmosphere. Obviously, this pyrolysis-rate law will cause a linear decrease of the regression rate when no other effects are considered.

Other minor contributions may come from the variation of the molar mass of the gas mixture coming from HTPB pyrolysis [6], resulting in a variation of the gas constant R for the mixture [which enters in the definition of the kinematic viscosity by law (56) and in the density calculation]. Finally, in [14], it is shown how the formulation of HTPB/GOX tends to operate at mixture ratios above the stoichiometric value (about 2.6) when considering an increase in the total pressure in the chamber. Although the data are quite scarce, it would be possible to hypothesize a simple linear pyrolysis-rate law, leading to a lowering of the rate of regression of the solid surface and of performance in general, with departure from the stoichiometric value of the oxidizer-fuel ratio, and a lower flame temperature. An analysis of sensitivity to the stoichiometric factor for the oxygen consumption at the surface is also present in the model.

Considering all the effects previously shown, using the law (35) with a decreasing preexponential factor, it is found, as stated before, that the regression rate is actually decreasing with increasing pressure. Figure 9 shows a comparison between the numerical results (and a simple fitting of them in the form $\dot{r} = qp^j$) and the trend predicted by Pennsylvania State Eq. (1). It is possible to see that, even allowing a pressure dependence of the preexponential factor, the dependence predicted by Eq. (1) is still more marked.

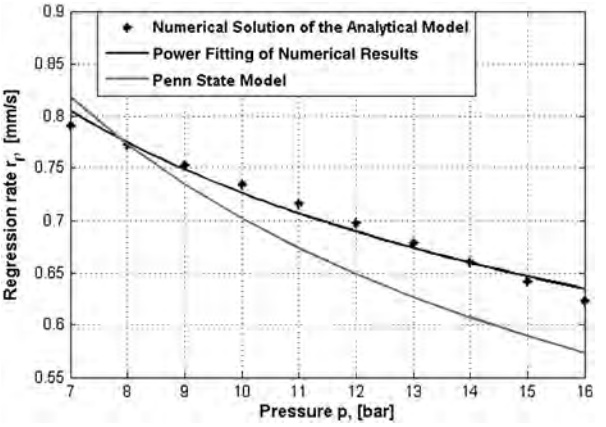

Fig. 9 Numerical results of the regression rate as a function of pressure.

As long as the experienced trend of the solid-fuel regression rate is greatly affected by the behavior of the preexponential constant B_{TD}, the major concern comes yet from another issue. Even allowing the use of partial experimental results for the setting of the input parameters of the model, we now must address the regression rate dependency on pressure through local effects at the interface. In other words, the Pennsylvania State University group [8] tried to fit the experimental values of $\dot{r}$ with a simple pyrolysis-rate law in the Arrhenius form for first-order reactions. The witnessed trend of $B_{TD}(p)$ is due to the global dependence on pressure of the hybrid combustor. A further modification of the pyrolysis-rate law would allow us to address the alleged dependence on pressure through specific local quantities at the surface. The "natural" choice is then to represent the partial density of oxygen in the rate law at the surface; in fact, the whole possibility of a pressure dependency has always been connected to the presence of oxygen below the flame zone. The goal now is to establish a more comprehensive law for the solid-fuel pyrolysis rate, which will replace Eq. (35) inside the analytical model. We look for a law in the form

$$\dot{r} = f(\rho_s Y_{o_s}, \rho_s Y_{f_s}, T_s) \tag{57}$$

where f is a fitted function of the oxygen partial density, the fuel partial density, and the temperature at the surface. All of those quantities will also depend on the values of pressure and of specific mass flux G_{ox}.

Comparison with Experimental Results and Construction of the Semi-Empirical Law

To find the proper function f, the experimental results from the Space Propulsion Laboratory will be used. Using the experimental values of the regression rate, the $\dot{r}$ unknown will be removed from the original system of unknowns and replaced by its experimental values for each pressure. Then, the simulation will be run, and with the found values of T_s, ρ_s, and Y_{o_s}, it will be possible to fit the new law. However, some modifications in the model need to be applied. Indeed, let us consider the experimental results in terms of instantaneous regression rate, presented earlier in Fig. 5. We consider that, in these steady-state experiments, both the pyrolysis rate and burning rate are directly proportional to the surface regression rate.

We will analyze pressure values from 7 to 16 bar because the results for the trials at 4 bar provide solutions only for a restricted range of G_{ox} values. We now consider G_{ox} to vary from 150 to 300 kg/(m^{2}s). For each value of G_{ox} we specify, for the four analyzed values of pressure, the regression rates, as shown in Table 1 for $G_{\text{ox}} = 250$ kg/(m^{2}s).

As said, it is not possible to simply take these values and use them as an input to the system. In fact, the model has a constant value of the velocity in input (set together with the Reynolds number and the respective boundary-layer thickness), whereas in the experiments, changing the value of pressure (and, hence, of the density) would

Table 1 Regression rate variation with pressure, $G_{ox} = 250$ kg/(m^{2}s)

p, bar	Ensemble $\dot{r}$, mm/s	Minimum $\dot{r}$, mm/s	Maximum $\dot{r}$, mm/s
7	0.748	0.702	0.802
10	0.759	0.703	0.823
13	0.740	0.713	0.791
16	0.726	0.699	0.821

imply a different value of the velocity because we are keeping the value of G_{ox} fixed. Hence, for each cycle, the following values must be recalculated: the value of the density of the gas ρ; the value of the horizontal velocity at the freestream by $u = G_{ox}/\rho$; the Reynolds number is actually fixed with G_{ox} because it will depend on the product ρu; and the value of $\nu_t = kx$ in the turbulent domains because it can be demonstrated that $k \propto \beta^2 u$. The value of ν_t can be computed by equating two times: the residence time that it would take a particle to get from the leading edge of the slab to an assigned value x, and the time to diffuse from the solid interface to the edge of the boundary layer $\delta = \delta(x)$. See Fig. 10.

$$t_1 \doteq t_2, \qquad t_1 = \frac{x}{u}, \qquad t_2 = \frac{\delta^2}{\nu_t} = \frac{\delta^2}{kx}$$

as

$$\delta = \beta x \Rightarrow \frac{x}{u} = \frac{\beta^2 x^2}{kx}$$

hence,

$$k \propto \beta^2 u$$

The solution is then refined with a few effects that were not taken into account in the original model: In fact, it did not reflect a change in the turbulent transport rates, due to temperature corrections on the effective Reynolds number when density and viscosity varied through the boundary layer. The representative Reynolds number was calculated using the density and the viscosity at the freestream. As the pressure increases, the surface temperature increases, causing a higher viscosity and a change in density near the surface. Taking averaged values of these quantities (between the freestream and the surface), the Reynolds number for the same velocity, pressure, and length would be lower. This would result in a lower value of the k factor. For this reason, the kinematic viscosity factor k at the freestream (previously set as $k = \beta^2 u_\infty$) will be remodeled as

$$k = \beta^2 u \frac{\rho_s + \rho_\infty}{2\rho_\infty} \tag{58}$$

to account for the density variation through the boundary layer, and the Reynolds number will be calculated using averaged values of density and viscosity

$$Re = \frac{(\rho_s + \rho_\infty/2)uD}{(\mu_s + \mu_\infty/2)} \tag{59}$$

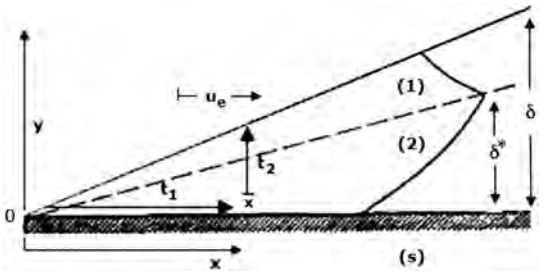

Fig. 10 Times used to compute ν_t.

Table 2 Example of pressure sensitivity of the different variables after corrections for $G_{ox} = 250$ kg/(m^{2}s)

p, bar	$\dot{r}$, mm/s	T_s, K	T_{fl}, k	Y_{f_s}	Y_{o_s}
7	0.748	983.8	2448.1	0.7739	3.83e − 3
10	0.759	984.3	2448.1	0.7744	1.61e − 5
13	0.740	1000.3	2488.3	0.7662	4.31e − 5
16	0.726	1014.1	2488.7	0.7592	3.91e − 5
p, bar	$Y_{o_{fl}}$	γ	$\rho_s Y_{o_s}$	$\rho_s Y_{f_s}$	ρ_s
7	1.86e − 2	0.0840	1.9e − 2	3.94	5.10
10	4.83e − 3	0.0838	1.2e − 4	5.52	7.13
13	4.71e − 3	0.0838	3.8e − 4	6.84	8.83
13	4.52e − 3	0.0838	4.1e − 4	8.06	10.61

These corrections bring the results shown in Table 2 for the value of $G_{ox} = 250$ kg/(m^{2}s). This solution, other than the experimental values of $\dot{r}$ taken from the Space Propulsion Laboratory program, does not present any other empiricism.

The new law will consider that the presence of oxygen will increase the pyrolysis rate (and has then a positive sign). The effect of recombination will also be taken into account: As the pressure goes up, we expect an increase in recombination processes. For this reason, an unknown percentage of the partial density of the fuel is subtracted in the new law.

Finally, the effect of the change in the activation energy from the inert case to the oxidized one is also considered in the new law.

The relation will then assume the form, slightly more complicated than Eq. (35),

$$\dot{r} = A(c + (\rho_s Y_{o_s})^n) \exp\left(-\frac{E_1}{T_s}\right) - B \exp\left(-\frac{E_2}{T_s}\right) - C(\rho_s Y_{f_s}) \tag{60}$$

where A, c, n, B and C will be fitted using a least-squares method for nonlinear equations; E_1 and E_2 are in Kelvin, B is in meters per second, C is in (meters to the fourth power per kilogram per second), n is a number, and c and A units are derived from the power of the partial density of oxygen.

The first term is accounting for an increment in the pyrolysis rate, due to the presence of oxygen in the system. The value of E_1 (activation energy divided by the gas constant, here ≈1200 K) is set to a value lower than the one for the inert case (here $E_2 \approx 2500$ K), because Pennsylvania State University's experiments [8] (from which the value of E_1 is taken) demonstrate that the presence of

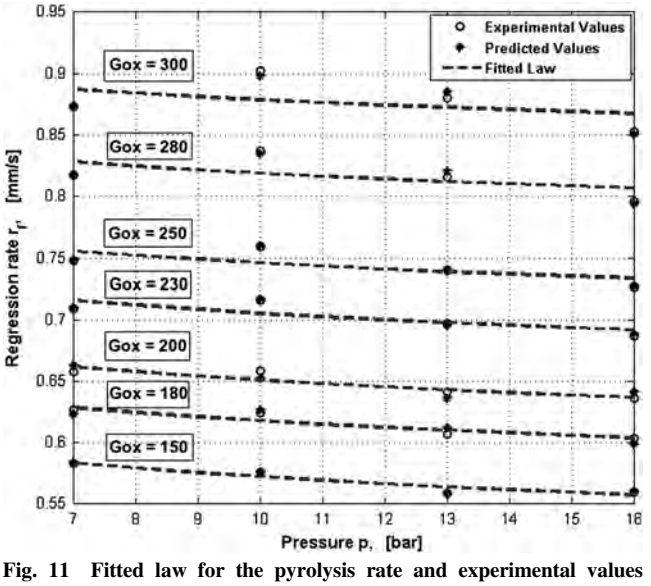

Fig. 11 Fitted law for the pyrolysis rate and experimental values comparing fitted vs. experimental values for the solid-fuel regression rate.

Table 3 Percentage error for regression rate at different values of the oxidizer specific mass flux G_{ox} and pressure p

	$G_{ox} = 150$	$G_{ox} = 180$	$G_{ox} = 200$	$G_{ox} = 230$	$G_{ox} = 250$	$G_{ox} = 280$	$G_{ox} = 300$
$p = 7$	8.307	4.889	6.397	5.186	4.128	1.766	−0.586
$p = 10$	2.197	2.680	2.966	2.605	1.832	−0.474	−3.147
$p = 13$	−4.301	−2.097	−0.949	−0.047	−0.028	−1.272	−3.242
$p = 16$	−6.971	−5.153	−3.873	−2.711	−2.306	−2.661	−3.851
Average error	−0.192	0.080	1.135	1.258	0.906	−0.66	−2.706

oxygen will enhance the pyrolysis (hence, a lower activation energy, around half of the inert one given by Chiaverini et al. [13]). Hence, it is, in a sense, like accounting for the oxygen increment twice: once through an increased preexponential constant $[c + (\rho_s Y_{o_s})]$ and once through a decreased value of E. Considering now a fixed value of $T_s \geq 1000$ K, the first exponential term (with E_1) is around three times bigger than the second term with E_2. The sense of subtracting that value represents a sort of rebalancing of a too-high increase caused by the first term. The contribution of the partial density of oxygen is presented summed to a constant c. This device is used so that, when considering $Y_{o_s} = 0$ (as in any case in which no oxygen is present in the formulation), the regression rate will not become negative. The last term again is used to account for recombination effects.

Considering a separate fitting for different values of G_{ox}, we see in Fig. 11 that the chosen law of Eq. (60) is suitable to fit the pyrolysis rate in all the cases.

We now want to fit the law using all of the available data, having a single fitting for all the possible values of p and G_{ox}. Combining all of the results together in a nonlinear system in the form

$$\dot{r} - \left[A(c + (\rho_s Y_{o_s})^n) \exp\left(-\frac{E_1}{T_s}\right) - B \exp\left(-\frac{E_2}{T_s}\right) - C(\rho_s Y_{f_s})\right] = 0 \tag{61}$$

where $\dot{r}$ is now a column vector containing all of the experimental results for the different values of G_{ox} and p, with $\rho_s Y_{o_s}$, T_s, and $\rho_s Y_{f_s}$ also column vectors, it is possible to get the values for the fitting constants:

$$A = 9.811e-3, \qquad c = 1.562e-2,$$
$$n = 2.781e-4 \quad B = 3.048e-2, \qquad C = 6.314e-7$$

Table 3 shows the percentage error for regression rate at each value of G_{ox} kg/(m^2 s) and at the different pressures. The error is always less than 10%. The highest values of the error are found for low values of the specific mass flow G_{ox}. This means that the model (and the fitting) tends to be more accurate for high values of the Reynolds number, that is to say, for the first instants of functioning of the combustor. Successive instants of time are more poorly approximated.

Conclusions

A new comprehensive model for the diffusive flame of the hybrid-rocket engine was developed. The main difference with respect to the previous models is that, here, the possible presence of oxygen below the flame zone is considered. Two different points of view must be taken into account: 1) how the diffusion of oxygen below the flame affects the operating system, and 2) how the pressure variation affects the diffusion of oxygen and, hence, the regression rate.

Regarding the first point, two effects are experienced. The presence of oxygen at the surface is theoretically responsible for the enhancement of the pyrolysis rate of the solid fuel. This comes from the observation that the presence of oxygen near the fuel surface can enhance the heterogeneous reactions and the overall pyrolysis process because the surface, in the presence of oxygen, will be already reacting with the surrounding oxygen when starting the pyrolysis process. The second effect is instead a more global consideration on the operating conditions in the presence of oxygen. From the reported results, it is possible to see that, when the oxygen is allowed to diffuse below the flame zone, a decrease in the flame temperature, together with an increase in the ordinate of the flame position, is witnessed. As was explained, having some oxygen diffuse below the flame, the amount consumed in the combustion is lower, causing a decrease in the flame temperature as more energy is gained at the surface instead. This will affect in a negative way the thermal energy feedback to the surface, yielding a lower surface temperature due to the decreased value of the flame temperature and to the increased distance between the two reacting zones. This effect is, however, slight, and the net result is still an increase in the regression rate due to the enhancement of the chemical kinetics caused by the presence of oxygen.

The second point investigates how the pressure affects the amount of oxygen that is diffusing below the flame. The research shows that an increase in the total pressure will cause a nonmonotonic trend in the behavior of the mass fraction of oxygen both at the surface and at the flame, causing a consequential nonmonotonic behavior of the regression rate. The effects are, however, slight, and this allows the authors to deduce that no evident dependence of the regression rate on the chamber total pressure is witnessed under the explored operating conditions.

The following points are then considered achieved by the present work:

1) A model was created that addresses the variation of pressure for the diffusion flames of the hybrid rocket. Two versions of the model are examined: the first one forcing the mass fraction of oxygen to be null at the wall ($Y_{o_{fl}} \neq 0$ and $Y_{o_s} = 0$) and the second one letting it vary ($Y_{o_{fl}}, Y_{o_s} \neq 0$).

2) A semi-empirical law for the pyrolysis rate was developed that will consider its direct dependence on pressure, which is determined by clarifying, through the model, the indirect dependence on pressure, which is traced through the variation of local quantities at the solid surface, such as temperature and species concentrations.

Still, the model presents a substantial simplification from both the fluid dynamic, thermodynamic, and chemical perspectives. A refinement of the description of the velocity and temperature fields inside the boundary layer should also reduce the percentage error. Further numerical solutions may be performed starting from the results of this simplified model; more robust and exact simulations can benefit from the use of this first analysis as a guide. Finally, note that the geometry used for the analytical model is a flat slab, whereas the experiments used a cylindrical sample. The Reynolds number of the analytical model was defined using a characteristic length equal to the initial port diameter. The initial Reynolds numbers in the two geometries equal each other. However, they should become unequal for the following time because the port diameter varies with time. The model keeps that characteristic length fixed but future refinements could address that matter.

Acknowledgments

The authors wish to thank C. Paravan, A. Sossi, and E. Duranti for significant help in experimental data handling and reduction. The authors also thank the anonymous reviewers who helped better express some of the ideas contained in this work.

References

[1] Marxman, G. A., and Wooldridge, C. E., "Fundamentals of Hybrid Boundary Layer Combustion," AIAA Paper 1963-5005, 1963.

[2] Gilbert, M., and Marxman, G. A., "Turbulent Boundary Layer Combustion in the Hybrid Rocket," *Ninth International Symposium on Combustion*, The Combustion Inst., Pittsburgh, PA, 1963, pp. 371–383.

[3] Price, C. F., and Smoot, L. D., "Regression Rate Mechanisms of Nonmetalized Hybrid Fuel Systems," *Aerospace Sciences Meeting*, AIAA Paper 1965-56, 1965.
[4] Price, C. F., and Smoot, L. D., "The Pressure Dependence of Hybrid Fuel Regression Rates," *AIAA Journal*, Vol. 5, No. 1, 1967, pp. 102–106. doi:10.2514/3.3914
[5] Sutton, G. P., and Biblarz, O., *Rocket Propulsion Elements*, 7th ed., Wiley, New York, 2001.
[6] Arisawa, H., and Brill, T. B., "Flash Pyrolysis of HTPB I: Analysis and Implications of the Gaseous Products," *Combustion and Flame*, Vol. 106, Nos. 1–2, 1996, pp. 131–143. doi:10.1016/0010-2180(96)00253-2
[7] Arisawa, H., and Brill, T. B., "Flash Pyrolysis of HTPB II: Implications of the Kinetics to Combustion of Organic Polymers," *Combustion and Flame*, Vol. 106, No. 1, 1996, pp. 144–154. doi:10.1016/0010-2180(95)00254-5
[8] Risha, G. A., Harting, G. C., Kuo, K. K., Peretz, A., Koch, D. E., Jones, H. S., and Arves, J. P., "Pyrolysis and Combustion of Solid Fuels in Various Oxidizing Environments," *Joint Propulsion Conference*, AIAA Paper 1998-3184, 1998.
[9] Smoot, L. D., Price, C. F., and Mihlfeith, C. M., "The Pressure Dependence of Hybrid Fuel Regression Rates," *Aerospace Sciences Meeting*, AIAA Paper 1966-113, 1966.
[10] Altman, D., "Highlights in Hybrid Rocket Propulsion," *International Workshop on Combustion and Propulsion In-Space Propulsion*, edited by DeLuca, L. T., Sackheim, R. L., and Palaszewski, B. A., Vol. 10, Grafiche, Bergamo, Italy, 2005, pp. 17.1–17.21.
[11] Karabeyoglu, M. A., Zilliac, G., Cantwell, B. J., De Zilwa, S., and Castelluci, P., "Scale-up Tests of High Regression Rate Liquefying Hybrid Rocket Fuels," *Joint Propulsion Conference*, AIAA Paper 2003-1162, 2003.
[12] Sirignano, W. A., "A General Superscalar for the Combustion of Liquid Fuels," *Proceedings of the Combustion Institute*, The Combustion Inst., Pittsburgh, PA, 2002, pp. 535–542.
[13] Chiaverini, M. J., Harting, G. C., Lu, Y., Kuo, K. K., Peretz, A., Jones, H. S., Wygle, B. S., and Arves, J. P., "Pyrolysis Behavior of Hybrid Rocket Solid Fuels Under Rapid Heating Conditions," *AIAA Journal*, Vol. 15, No. 6, 1999, pp. 888–895. doi:10.2514/2.5512
[14] Strand, L. D., Jones, M. D., and Ray, R. L., "Characterization of Hybrid Rocket Internal Heat Flux and HTPB Fuel Pyrolysis," AIAA Paper 1994-2876, 1994.

S. Son
Associate Editor